第51卷第8期 中国科学技术大学学报 Vol. 51, No. 8
2021年8月 JOURNAL OF UNIVERSITY OF SCIENCE AND TECHNOLOGY OF CHINA Aug. 2021
Received: 2021-04-07; Revised: 2021-04-29 doi:10.52396/JUST-2021-0101

Highly perfluorocarbon loading efficiency of polymer biomimetic nanoparticle encapsulated by erythrocyte membrane to improve tumor phototherapy

SUN Xun, YU Yue*
Department of Gastroenterology, The First Affiliated Hospital of USTC(Anhui Provincial Hospital), Division of Life Sciences and Medicine, University of Science and Technology of China, Hefei 230001, China
* Corresponding author. E-mail: yuyuemd@ustc.edu.cn

Abstract: Photodynamic therapy (PDT) is an emerging treatment method that relies on oxygen. However, due to the insufficient oxygen supply to the blood vessels at the tumor site, the hypoxic microenvironment greatly inhibits the therapeutic effect of PDT. Therefore, how to alleviate the tumor hypoxia is the key issue of the development of PDT. Perfluorocarbon is a compound that can effectively carry oxygen and is one of the commonly used blood substitutes. We carry oxygen and photothermal drug Indocyanine Green (ICG) through PFC (bromide hepta-fluorooctane) nanoparticles, and coat the particles with red blood cell membranes for bionic camouflage to reduce the uptake of particles by macrophages, improve the circulation capacity of the particles and enhance the ability of the drug to accumulate in the tumor. In addition, we combine PDT to effectively alleviate the hypoxia in the tumor microenvironment, enhance the photodynamic effect, and provide new strategies for cancer therapies.
Keywords: drug delivery system; cancer therapy; photothermal therapy; photodynamic therapy
CLC number: R730.5 **Document code**: A

1 Introduction

Tumor is one of the urgent public health problems in the world today, but there are still some problems in conventional therapies (such as surgery[1,2], chemotherapy[3], immunotherapy[4], etc.) that makes the treatment effect unsatisfactory. The photodynamic therapy (PDT) has been brought to the fore by data as the rapid development of the tumor treatment[5,6]. The mechanism of PDT is to use light to decompose the photosensitizer to produce free radicals, and then the free radicals react with triplet oxygen to produce singlet oxygen, which finally leads tumor cell to death[7,8]. However, the proliferation rate of tumor cells is much greater than that of vascular endothelial cells in the process of the tumor growth, resulting in abnormal blood vessels in the tumor and the formation of a hypoxic microenvironment[9]. Generally, the area close to the blood vessel has higher oxygen content, while the deep part of the tumor far away from the blood vessel is highly hypoxic. This hypoxic microenvironment makes it difficult for the photodynamic therapy to produce enough reactive oxygen species (ROS) to treat tumors. Therefore, increasing the oxygen content of the tumor microenvironment and alleviating hypoxia is an important way to enhance the photodynamic therapy.

In order to solve the problem of lack of oxygen in the tumor microenvironment, methods such as carrier delivery[10], improved vascular perfusion[11], and decomposition of hydrogen peroxide[12] are generally used. Among them, the perfluorocarbon called "white blood" is one of the common blood substitutes as a carrier with high-efficiency oxygen carrying capacity[13].

However, there are multiple physiological barriers such as blood barriers, tissue barriers, and intracellular transport barriers during the delivery process[14]. In order to reduce the impact of multiple physiological barriers on the delivery efficiency, PLGA (polylactic acid-glycolic acid copolymer)[15,16] with good biocompatibility is generally used as nano-carriers, and the special characteristics of nano-scale are used to extend the circulation time in the body. Our groups have constructed a variety of nano-drug carriers such as the gold[17] and graphdiyne oxide[18].

Herein, we used oxygen-carrying PFC (bromide hepta-fluorooctane) nanoparticles to relieve hypoxia in the tumor microenvironment, and combined with the

Citation: Sun Xun, Yu Yue. Highly perfluorocarbon loading efficiency of polymer biomimetic nanoparticle encapsulated by erythrocyte membrane to improve tumor phototherapy. J. Univ. Sci. Tech. China, 2021, 51(8): 598-608.

carried ICG to improve the photodynamic effect. In addition, the erythrocyte membrane was used to coat the nanoparticles to reduce the uptake of particles by macrophages, reduce the toxic and side effects of drugs, and increase the accumulation of drugs in tumors. The use of red blood cell membranes for bionic camouflages can reduce the uptake of particles by macrophages through the combination of CD47 on the cell membrane surface and SIRPα of macrophages[19], which can effectively extend the circulation time of the nanomedicine in the body and the accumulation of tumors.

2 Materials and methods

2.1 Materials

Lactide (LA) and Glycolide (GA) were purchased from Ji'nan Daigang Biomaterial Co., Ltd. Aminoethanol (EA), sodium acid carbonate, tetrahydrofuran, diethyl ether, dimethyl sulfoxide (DMSO) and dichloromethane (DCM) were purchased from Sinopharm Chemical Reagent Co., Ltd. Perfluorodecalin and histidine were purchased from Sigma-Aldrich. Di-tert-butyl dicarbonate, Trifluoroacetic acid (TFA), N-Hydroxysuccinimide (NHS), N, N-Diisopropylethylamine (DIPEA) and Pentadecafluorooctanoic acid (PFOA) were purchased from Aladdin. Tin(II)-2-Ethylhexanoate was purchased from Tokyo Chemical Industry (TCI). 1-(3-Dimethylaminopropyl)-3-ethylcarbodiimide hydrochloride (EDC) was purchased from J&K Chemicals.

2.2 Synthesis of EA-Boc

25 mL THF, 50 mL water, amino-ethanol (56.1 g, 0.92 mol) and sodium acid carbonate (134.6 g, 1.6 mol) were added in a three-necked flask in order. The Di-tert-butyl dicarbonate diluted in THF was dropped in the solution at 0 ℃. After adding, the mixture reacted overnight at the room temperature. After reaction, the product was filtered. Thereafter, THF was removed by the rotary evaporator. The solution was extracted by diethyl ether three times. After removal of solvent in a vacuum, the thick liquid was the product. The synthesis route is shown in Scheme S1. The ^{1}H NMR spectrum is shown in Figure S1.

2.3 Synthesis of PLGA

LA (7.846 g), GA (2.075 g) and EA-Boc were added in a dry flask. The mixture was stirred at 130 ℃. After the solid was molten, 10 mg Tin(II)-2-Ethylhexanoate was added in solution. The system became sticky gradually. After 2 h, the reaction finished and the product was precipitated in the diethyl ether. The synthesis route is shown in Scheme S2. The ^{1}H NMR spectrum is shown in Figure S2. The GPC is shown in Figure S3.

2.4 Synthesis of PLGA-NH_2

PLGA and TFA were dissolve in DCM. The solution was stirred at room temperature for 1 h. Subsequently, DIPEA was dropped in the solution until there was no smoke. The mixture was dialyzed against the deionized water. And then, the solution was lyophilized to obtain PLGA-NH_2. The ^{1}H NMR spectrum is shown in Figure S4.

2.5 Synthesis of FPLGA

PFOA (2.07 g, 0.005 mol), EDC (1.917 g, 0.01 mol) and NHS (1.15 g, 0.01 mol) were dissolved in DCM. After stirred for 3 h, the solution was added with PLGA-NH_2 (5 g, 0.001 mol). And then, the reaction finished after another 48 h. Subsequently, the product was precipitated in the diethyl ether. The synthesis route is shown in Scheme S4. The ^{19}F NMR spectrum is shown in Figure S5.

2.6 Preparation of PFC@FPLGA nanoparticle

PFC@FPLGA nanoparticle was prepared by doubling the emulsion (water/oil/water) solvent evaporation[19]. Briefly, 12.5 mg FPLGA and 12.5 mg PEG-b-PLGA were dissolved in DCM along with 50 μL PFC, in which 5 mL 5% PVA solution (w/v) was then added. After well stirred, the mixture was sonicated in the ice water bath for 5 min totally, with 5 s on, 2 s off, 70% power output. Then another 1.5 mL PVA solution was added to homogenize the emulsion, that was stirred open at the room temperature for 4 h to vaporize DCM. The product was centrifuged at 15000 r/min for 30 min at 4 ℃. And then it was washed several times with the ultrapure water to remove PVA. PFC@FPLGA nanoparticle was re-suspended in the de-ionized water.

2.7 Preparation of RBCM vesicles

The RBCM vesicles were obtained by extrusion approaches[20]. Briefly, freshly heparinized blood was centrifuged at 4000 r/min for 10 min at 4 ℃. And then, the precipitation was re-suspended in hypotonic buffer for 30 min at 37 ℃. The mixture was centrifugated at 9000 r/min for 10 min at 4 ℃ to separate the hemoglobin.

2.8 Preparation of PFC@$RBCM_{ICG}$ nanoparticle

PFC@FPLGA nanoparticle was dissolved in 1 mL deionized water, in which there was 100 μL ICG aqueous solution (1 mg/mL) and 100 μL RBCM. The mixture was stirred overnight at 4 ℃. PFC@$RBCM_{ICG}$ nanoparticle was obtained by being centrifuged at 15000 r/min for 30 min at 4 ℃ and re-suspended in PBS.

2.9 Characterization of nanoparticle

The morphology of the nanoparticle was observed by the transmission electron microscope (TEM) (JEM-2011). The size and zeta potential for nanoparticles was measured by dynamic light scattering (Nano-zs90, NANERN).

The PFOB encapsulation efficiency was measured by ^{19}F NMR on a BUKER-300 (300 MHz) spectrometer.

In brief, the nanoparticle was dissolved in 1 mL $CDCl_3$ in which 5 μL TFA was added as the external standard. The total volume of PFOB in the nanoparticle was determined by the peak at −190 ppm corresponding to the CF_2Br group and normalization by the area of the TFA peak at −75 ppm. Besides, different volumes of PFC (5 μL, 10 μL, 20 μL, 25 μL) were quantitied in the same way.

$$\text{PFC Drug Loading Efficiency (DLE)} = \frac{\text{Mass of PFC in PFC@RBCM}_{ICG}}{\text{Mass of Free PFC}}$$

$$\text{PFC Drug Loading Content (DLC)} = \frac{\text{Mass of PFC in PFC@RBCM}_{ICG}}{\text{Mass of FPLGA}}$$

The ICG encapsulation efficiency was measured by the UV spectrophotometry on an Agilent Technologies (Cary 60) spectrometer. Different concentration of ICG was measured as the standard curve.

$$\text{ICG Drug Loading Efficiency (DLE)} = \frac{\text{Mass of ICG in PFC@RBCM}_{ICG}}{\text{Mass of Free ICG}}$$

$$\text{ICG Drug Loading Content (DLC)} = \frac{\text{Mass of ICG in PFC@RBCM}_{ICG}}{\text{PFC@RBCM}_{ICG}}$$

Before the measurement of dissolved oxygen, 1 mL PFC@ $RBCM_{ICG}$ solution was ventilated oxygen for 30 min and 5 mL deionized water was added into a closed beaker, which was purged with nitrogen to remove the dissolved oxygen. The oxygen concentration in the beaker was measured with a Foxy Fospor-R oxygen sensor (Ocean Optics, Dunedin, FL) before and after adding the PFC@ $RBCM_{ICG}$ solution. In addition, PFC@ $RBCM_{ICG}$ solution without oxygenation, H_2O with oxygenation, H_2O without oxygenation and different concentration PFC@ $RBCM_{ICG}$ solution with oxygenation were measured with the same method.

In vitro photothermal properties of PFC@ $RBCM_{ICG}$ were evaluated by measuring the photothermal conversion efficiency. PFC@ $RBCM_{ICG}$ with different concentration (0, 0.5, 1.0, 2.0, 3.0 μg/mL) was irradiated by NIR laser with different power (0, 0.5, 1.0, 1.5, 2.0 W/cm^2). The temperature was recorded by an infrared thermal-imaging camera (Fotric 226, China).

In vitro photodynamic properties of PFC@ $RBCM_{ICG}$ were evaluated by DPBF assay. Briefly, 10 μL PFC@ $RBCM_{ICG}$ solution or ICG solution with the same ICG concentration was mixed with 50 μL DPBF solution in a 1 mL centrifuge tube which was irradiated with a NIR laser (808 nm) at the power density of 1.0 W/cm^2 for different time intervals. After irradiation, the mixture was measured by the absorbance with UV spectrophotometry.

2.10 Cell culture and in vitro cytotoxicity assays

Murine breast cancer cell line 4T1 cells were obtained from Shanghai Institute of Cells, Chinese Academy of Science and cultured in the glucose medium (DMEM, Gibico) at a mixed atmosphere of 5% CO_2 at 37 ℃.

To research the cytotoxicity of PFC@ $RBCM_{ICG}$ nanoparticle in vitro, 3-(4,5-dimethylthiazol-2-yl)-2,5-diphenyltetrazolium (MTT) assay was used to assess the cytotoxicity of PFC@ $RBCM_{ICG}$ nanoparticle and ICG to 4T1 cells. Briefly, 4T1 cells were seeded in 96 well plates at the density of 5000 cells per well (n=6). When the cultured cells reached 80% confluency, the plates were added with PFC@ $RBCM_{ICG}$ nanoparticles and ICG at various concentrations (0, 0.15, 0.30, 0.60, 1.25, 2.5, 5.0, 10.0 μg/mL). After incubation for 24 h, the medium was replaced by the fresh medium containing 0.75 mg/mL MTT, and the medium containing MTT was carefully removed and replaced by 100 μL DMSO after 4 h. And then, the plates were gently shaken by the shaker in the night for 10 min. The absorbance of each well was measured with a microplate reader (Molecular Devices, SpectraMax M2e, USA).

2.11 In vitro photodynamic therapy and photothermal ablation against cancer cells

To study the therapeutic effects of PFC@ $RBCM_{ICG}$, 4T1 cells were seeded in a 96-well plate at the density of 6000 cells per well (n = 4). When the cultured cells reached 75% confluency, the plates were flushed with humidified 1% O_2, 5% CO_2 and 94% N_2 (hypoxia chamber). After incubated in 37 ℃ for 4 h, the cells were incubated with the fresh medium containing PFC@ $RBCM_{ICG}$ and PLGA@ $RBCM_{ICG}$ nanoparticles at the concentrations of 2.5 and 5.0 μg/mL. And then, the plates were incubated for another 4 h, 4T1 cells received different treatments. As for the PDT treatment only, the plates were put in ice water. 1 μmol/L histidine was added in each well to block the ROS generation for the PTT treatment only. And then, the cells were incubated for 12 h. Finally, MTT assay was used to evaluate the therapy efficiency of nanoparticles.

2.12 Intracellular ROS generation

In order to study the enhanced ROS generation of PFC@ $RBCM_{ICG}$, six groups were divided (PBS, Laser, PLGA@ $RBCM_{ICG}$, PFC@ $RBCM_{ICG}$, PLGA@ $RBCM_{ICG}$ @ O_2, PFC@ $RBCM_{ICG}$ @ O_2). The 4T1 cells were seeded on coverslips in 24-well plate at the density of 6×10^4 cells per well. When the cultured cells reached 80% confluency, the plates were aerated with hypoxia atmosphere (1% O_2, 5% CO_2, and 94% N_2). After being incubated in 37 ℃ for 4 h, the cells were incubated with the fresh medium containing

nanoparticles. And then, the 4T1 cells were incubated for another 4 h and irradiated by NIR laser (808 nm, 1.0 W/cm^2) for 5 min per well. Next, the cells were further incubated with the 10 μmol/L DCFH-DA (Beyotime, Nanjing, China), for 1 h at 37 ℃. Subsequently, the cells were washed with PBS and the nucleus were stained with DAPI. Finally, the fluorescence images were observed by CLSM.

2.13 Cellular hypoxia evaluation

To measure the hypoxia alleviation of PFC@RBCM$_{ICG}$, six groups were divided (PBS, Laser, PLGA@RBCM$_{ICG}$, PFC@RBCM$_{ICG}$, PLGA@RBCM$_{ICG}$@O$_2$, PFC@RBCM$_{ICG}$@O$_2$). The 4T1 cells were seeded on coverslips in 24-well plate at the density of 6×10^4 cells per well. When the cultured cells reached 75% confluency, the plates were aerated with the hypoxia atmosphere (1% O$_2$, 5% CO$_2$, and 94% N$_2$). After being incubated in 37 ℃ for 4 h, the cells were incubated with fresh medium containing nanoparticles. And then, the 4T1 cells were incubated for another 4 h. Next, the cells were incubated with the pimonidazole hydrochloride for 1 h at 37 ℃. Subsequently, the cell nuclei and hypoxia were stained by DAPI and FITC-Mab1. Finally, the fluorescence images were observed by CLSM.

2.14 Cellular uptake

In order to verify the ability of RBCM to suppress the uptake of macrophage, PFC@RBCM and PFC@FPLGA nanoparticles were incubated with RAW264.7 cells obtained from Affiliated Hospital of Anhui Medical University. Briefly, RAW264.7 cells were seeded on coverslips in 24-well plate at the density of 6×10^4 cells per well. When the cultured cells reached 75% confluency, the plates were aerated with the hypoxia atmosphere (1% O$_2$, 5% CO$_2$, and 94% N$_2$). After being incubated in 37 ℃ for 4 h, the cells were incubated with fresh medium containing nanoparticles. And then, collecting the RAW264.7 cells and resuspending with PBS. Finally, the uptake of macrophage was measured with flow cytometry and CLSM. The uptake of 4T1 cells was operated with the same method.

2.15 Pharmacokinetic study of PFC@RBCM$_{ICG}$

Female Balb/c mice were purchased from Anhui Medical University (n = 3). In order to study the pharmacokinetic of nanoparticles, the mice were injected with PFC@RBCM and PFC@FPLGA nanoparticles labeled by DID. The blood, which was collected 30 μL from each mouse at different time interval (0.5 h, 1 h, 2 h, 4 h, 8 h, 12 h, 24 h, 48 h post-injection), was added in a black 96-well plate. And then, the fluorescence intensity of each well was measured with the IVIS Spectrum Imaging System.

2.16 In vivo antitumor efficacy of PFC@RBCM$_{ICG}$

As for the in vivo antitumor efficacy of PFC@RBCM$_{ICG}$ nanoparticles, 4T1 tumor-bearing mice were injected with different formulations (PBS, PFC@RBCM$_{ICG}$, PLGA@RBCM$_{ICG}$@O$_2$, PFA@RBCM$_{ICG}$@O$_2$) at an equivalent dose of 20.0 mg PFA per kg mouse weight when the tumor volume reached 100 mm^3 (n = 4). The NIR laser (808 nm, 1.0 W/cm^2) was applied to irradiate the tumor in the next day, and the tumors were measured every two days for 20 days. The tumor volume was measured by calipers and calculated: Tumor Volume = (Length) × (Width)^2×0.5.

2.17 In vivo distribution of PFC@RBCM$_{ICG}$

As for the in vivo distribution of PFC@RBCM$_{ICG}$ nanoparticles, 4T1 tumor-bearing mice (n = 3) were injected with PFC@RBCM and PFC@FPLGA nanoparticles labeled by DID. Subsequently, the fluorescence intensity of each mice was measured with the IVIS Spectrum Imaging System at different time intervals (1 h, 4 h, 12 h, 24 h, 48 h, 72 h post-injection).

2.18 Statistical analysis

The data was assessed by Graphpad prism 7 software (GraphPad, San Diego, CA) with Student's T-test method. Significant difference among group were assigned as $^*p<0.05$, $^{**}p<0.01$ and $^{***}p<0.001$, respectively. $^*p<0.05$ was considered statistically significant in all analyses (95% confidence level).

3 Results and discussions

3.1 Synthesis and characterization

The preparation of PFC@RBCM$_{ICG}$ nanoparticles is shown in Scheme 1. It consisted of red blood cell membranes (RBCM), indocyanine green (ICG), bromide hepta-fluorooctane (PFC) and fluorinated polyglycolide-lactide copolymer (FPLGA) compositions.

Among them, RBCM was separated and extracted from the blood of mice, which can reduce the uptake of nanoparticles by macrophages and increase the circulation time in the body. As a photosensitizer approved by the FDA for clinical use, ICG has excellent photothermal and photodynamic properties[21]. FPLGA was prepared by esterification reaction between PLGA (LA and GA ring-opening polymerization) and perfluorooctanoic acid. The PFC, which has the function of relieving the tumor hypoxia microenvironment and enhancing the phototherapy function, was wrapped in FPLGA to form PFC@FPLGA nanoparticles by phacoemulsification. Finally, RBCM, ICG and PFC@FPLGA nanoparticles were stirred and mixed to prepare PFC@RBCMICG nanoparticles.

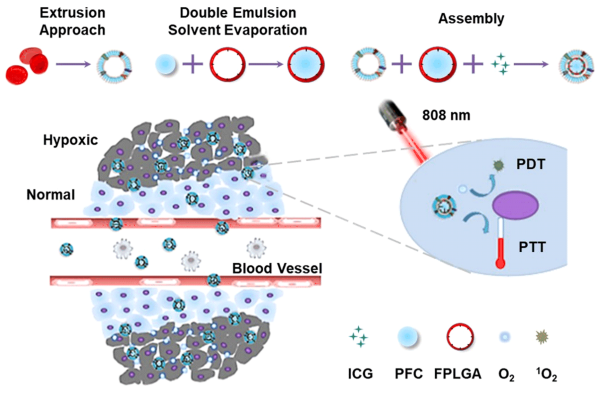

Scheme 1. The Strategy of PFC@ $RBCM_{ICG}$ to improve the tumor phototherapy. The extracted erythrocyte membranes are assembled into PFC@ $RBCM_{ICG}$ nanoparticles with the prepared PFC@ FPLGA nanoparticles and ICG. When the oxygen-carrying particles are swallowed by tumor cells, singlet oxygen is generated under the irradiation of NIR 808 nm laser. Therefore, PFC@ $RBCM_{ICG}$ NPs can treat tumors through the dual effects of PDT and PTT.

First, refer to the phacoemulsification method that our group has matured to prepare PFC @ FPLGA nanoparticles. Subsequently, we prepared PFC @ $RBCM_{ICG}$ nanoparticles with PFC@ FPLGA nanoparticles, RBCM, and ICG. As shown in Figure 1(a), the particle size of PFC @ $RBCM_{ICG}$ nanoparticles measured by a dynamic light scattering particle size analyzer was about 174 nm, which was 20 nm larger than PFC@ FPLGA nanoparticles. This difference in particle size indicated that the red blood cell membrane was well wrapped on the surface of the particles.

Furthermore, we observed through transmission electron micrographs that the surface of PFC@ $RBCM_{ICG}$ nanoparticles had a layer of the red blood cell membrane structure negatively stained with phosphotungstic acid (Figure 1(b)). From Figure 1(c), we can find that the potential of PFC@ FPLGA was −27 mV, while the particle size of PFC@ $RBCM_{ICG}$ nanoparticles was −15 mV, which was the same as the potential of RBCM.

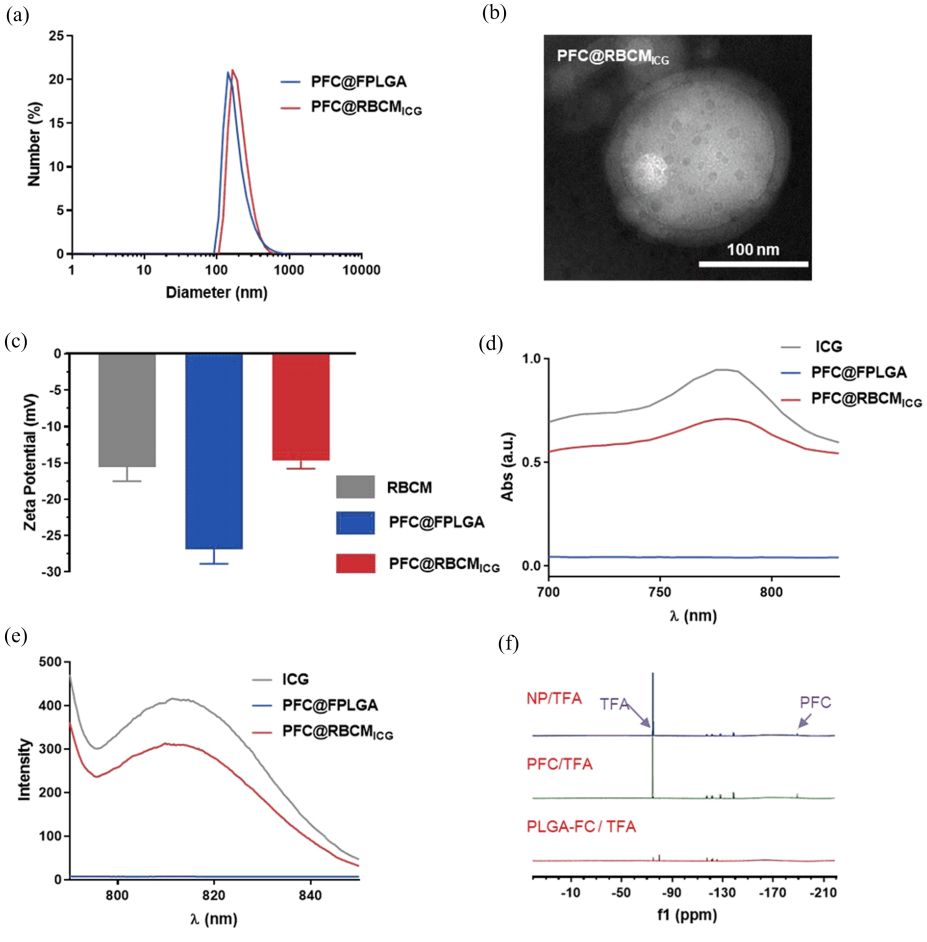

Figure 1. Physicochemical properties of the nanoparticles. (a) The particle size comparison of PFC@ FPLGA and PFC@ $RBCM_{ICG}$ with DLS. (b) TEM image of PFC@ $RBCM_{ICG}$. (c) The zeta potential of RBCM, PFC@ FPLGA and PFC@ $RBCM_{ICG}$. UV-Vis absorption spectra (d) and fluorescence spectra (e) of ICG, PFC@ $RBCM_{ICG}$ and PFC@ FPLGA. (f) Comparison of ^{19}F MNR between PFC@ $RBCM_{ICG}$ NPs, PFC and PLGA.

The result showed that the outer surface of PFC@$RBCM_{ICG}$ nanoparticles was covered by RBCM. Through the ultraviolet absorption spectrum and fluorescence excitation spectrum, we can find that PFC@FPLGA nanoparticles did not have obvious ultraviolet absorption or fluorescence, while PFC@$RBCM_{ICG}$ nanoparticles, which prepared by mixing PFC@FPLGA nanoparticles and ICG, have similar spectrums to ICG (Figure 1(d, e). The results showed that ICG was encapsulated in PFC@$RBCM_{ICG}$ nanoparticles. On the other hand, we measured PFC@$RBCM_{ICG}$ by ^{19}F NMR to have the same characteristic peak as PFC at −187 ppm, indicating that PFC was well encapsulated in PFC@$RBCM_{ICG}$ nanoparticles (Figure 1(f)).

It has been widely reported that perfluorocarbon can carry oxygen like hemoglobin. In order to evaluate the oxygen-carrying capacity of the prepared PFC@$RBCM_{ICG}$, we used oxygen sensors to measure the amount of oxygen released in different systems. According to the measured results, the PFC@PBCM that did not carry oxygen released very low oxygen, which was the same as H_2O. The oxygen released of PFC@PBCM@O_2 and H_2O@O_2 carrying oxygen was significantly increased, but PFC@PBCM@O_2 can be maintained for a long time, while the oxygen content of H_2O@O_2 decreased rapidly (Figure 2(a)). Therefore, the PFC@$RBCM_{ICG}$ of the equal volume has a higher oxygen carrying efficiency and is more stable than that of water. In addition, as the mass percentage of PFC increased, the oxygen concentration rose from 11.9 ppm to 15.8 ppm (Figure 2(b)).

Next, we used DPBF as an ROS probe to observe the changes in the absorbance of DPBF to verify the PDT performance of PFC@$RBCM_{ICG}$. Figure 2(c) showed that as the duration of the NIR laser irradiation on the nanoparticles increased, the absorbance gradually decreased after the reaction between DPBF and ROS. This result indicated that ROS was continuously produced in the system, which proved that PFC@$RBCM_{ICG}$ can increase the production of ROS and enhance the effect of PDT. On the other hand, we verified the PTT performance of PFC@$RBCM_{ICG}$. As shown in Figure 2(d), PFC@$RBCM_{ICG}$ can trigger a rapid heating effect under the irradiation of NIR laser (808 nm). The temperature rises with the increase of the laser power, and can reach 65.4 ℃ under the condition of 2 W/cm^2. It showed that PFC@$RBCM_{ICG}$ has both good photothermal and photodynamic performances.

3.2 The therapeutic effect of PFC@$RBCM_{ICG}$ on tumors

In order to prove that oxygen-carrying PFC@$RBCM_{ICG}$ can enhance tumor PTT treatment, we verified the ability of nanoparticles to relieve hypoxia and generate ROS.

First, we treated the cells with different nanoparticles (PLGA@$RBCM_{ICG}$, PFC@$RBCM_{ICG}$,

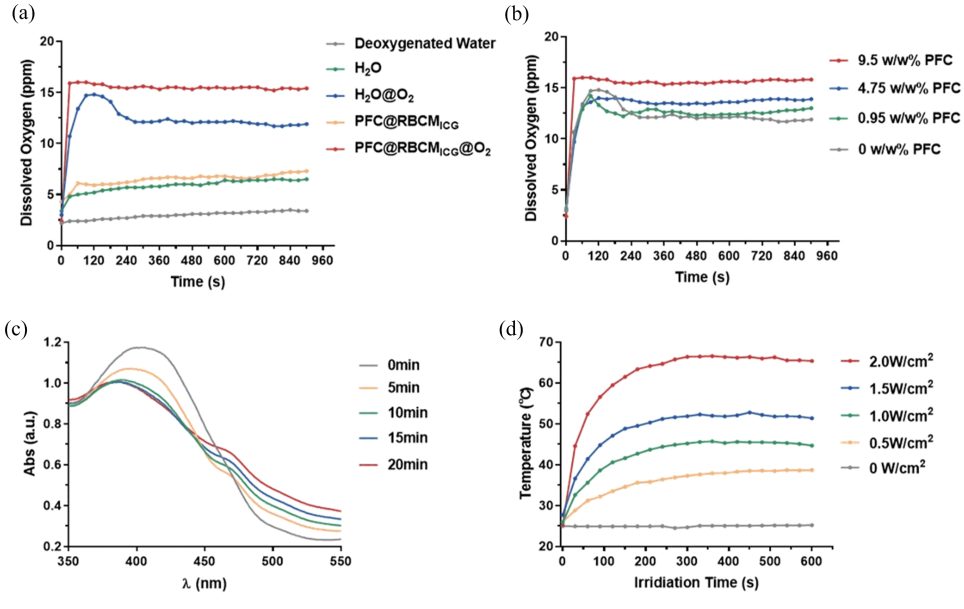

Figure 2. The ability of PFC@$RBCM_{ICG}$ for carrying oxygen, photodynamic and photothermal effects. (a) The change of the oxygen content in five solutions PFC@$RBCM_{ICG}$@O_2, H_2O@O_2, PFC@$RBCM_{ICG}$, H_2O and deoxygenated water over time. (b) The oxygen content in the solution changed with time, while the mass percentage of PFC was different. (c) Irradiated PFC@$RBCM_{ICG}$ with the NIR laser, and detected the UV absorption spectrum of the ROS probe (DPBF). (d) PFC@$RBCM_{ICG}$ temperature changed with time under different laser powers.

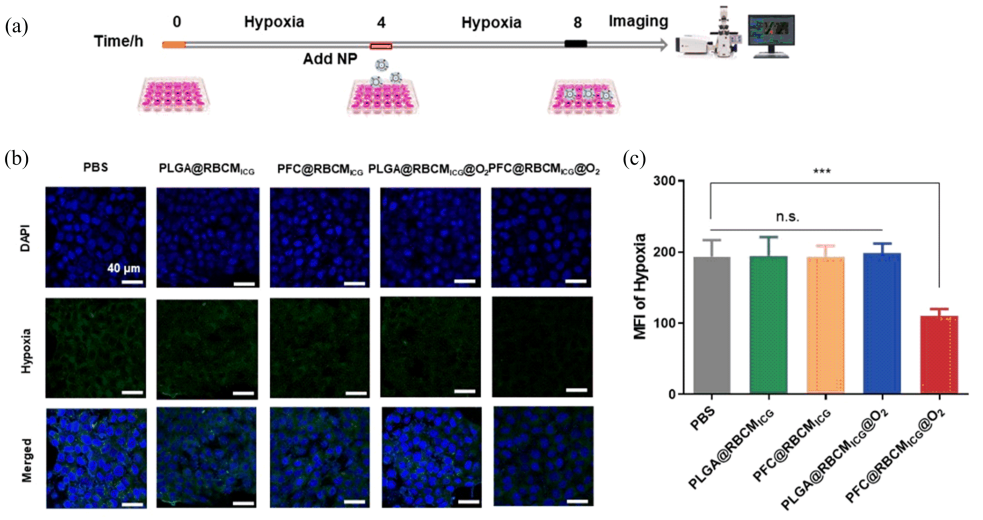

Figure 3. Hypoxia alleviation by PFC@ RBCM$_{ICG}$. A representative picture of 4T1 cells treated with different nanoparticles to detect oxygen content (a, b), and statistical mapping (c). Data are shown as mean ±SD (n=3) $^{*}p$<0.05, $^{**}p$<0.01, $^{***}p$<0.001.

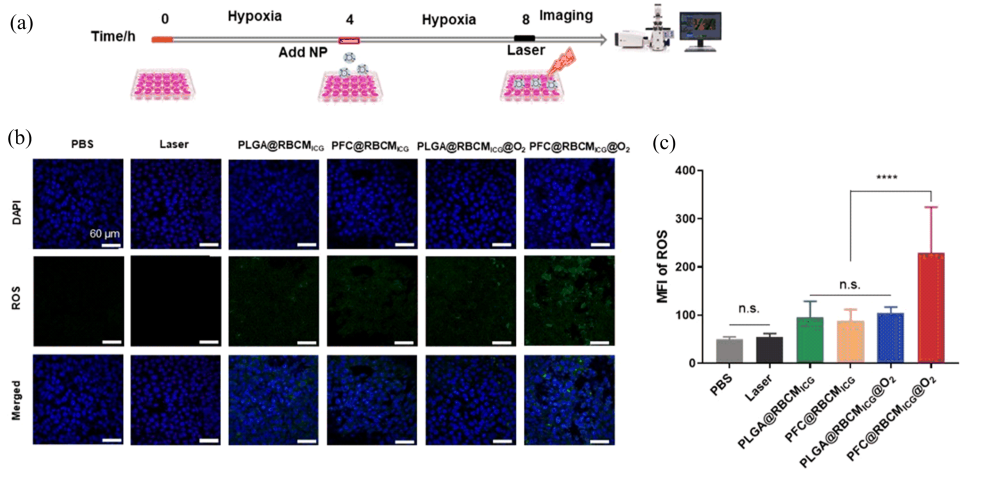

Figure 4. ROS generation by PFC@ RBCM$_{ICG}$. A representative picture of 4T1 cells treated with different nanoparticles to detect the ROS content (a, b), and statistical mapping (c). Data are shown as mean ±SD (n=3) $^{*}p$<0.05, $^{**}p$<0.01, $^{***}p$<0.001, $^{****}p$<0.0001.

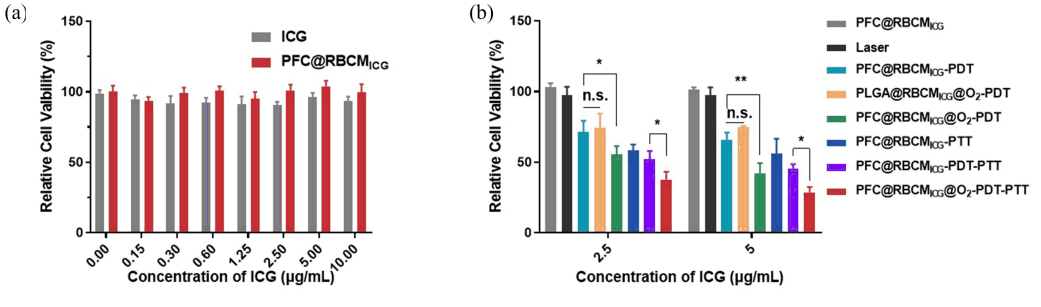

Figure 5. In vitro cytotoxicity of PFC@ RBCM$_{ICG}$. (a) Detect the cytotoxicity of PFC@ RBCM$_{ICG}$ by MTT method. (b) In vitro, the therapeutic effect of PFC@ RBCM$_{ICG}$ with and without oxygen on tumors. Data are shown as mean ±SD (n=3) $^{*}p$<0.05, $^{**}p$<0.01.

PLGA @ RBCM$_{ICG}$ @ O$_2$, PFC @ RBCM$_{ICG}$ @ O$_2$). Pimonidazole was used to detect oxygen and observed under the microscope (Figure 3(a)). As shown in Figure 3(b), the fluorescence of pimonidazole was

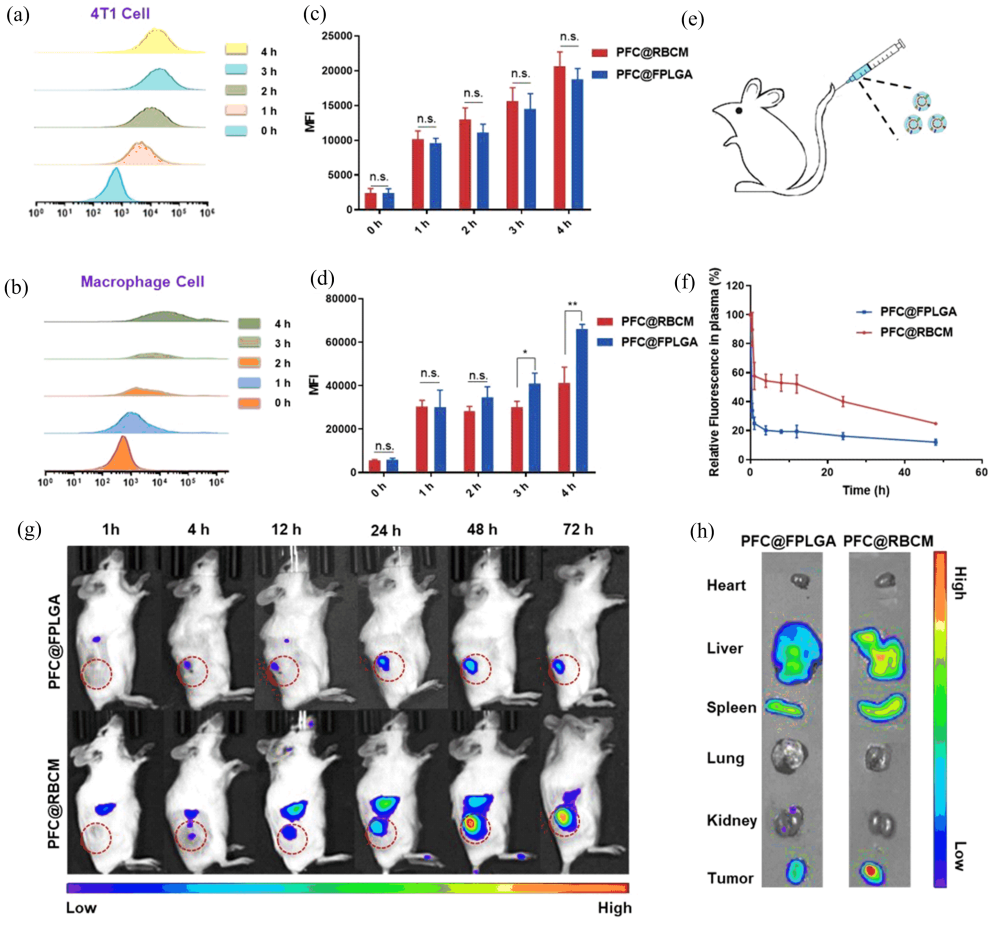

Figure 6. The pharmacokinetic properties and tumor accumulation of PFC@ RBCM. (a, c) Uptake of PFC@ RBCM and PFC@ FPLGA by 4T1 cells. (b, d) Uptake of PFC@ RBCM and PFC@ FPLGA by macrophages. (e) The mice were injected with nanoparticles through the tail vein. (f) The pharmacokinetic results of PFC@ RBCM and PFC@ FPLGA. (g, h) Accumulation of PFC @ RBCM and PFC@ FPLGA in mice. Data are shown as mean ±SD (n=3) $^{*}p$<0.05, $^{**}p$<0.01.

significantly reduced after treatment with oxygen-carrying PFC nanomedicine, and the MFI was only half of the others (Figure 3(c)). It showed that when the cells were treated with the nanoparticles, the oxygen content was significantly increased, which can effectively alleviate the hypoxic state of tumor cells.

On the other hand, we used DCFH-DA to detect the ROS concentration in cells treated with different conditions and observed under a microscope (Figure 4 (a)). The concentration of ROS in cells treated with PFC@ $RBCM_{ICG}$@ O_2 increased significantly, while the concentration of ROS in cells treated with other nanoparticles was lower (Figure 4(b, c)). As a result, the oxygen-carrying PFC nanomedicine can effectively increase the amount of ROS produced and enhance the effect of the photodynamic therapy.

The cytotoxicity of the nanoparticles was detected by the MTT method. When the ICG concentration was as high as 10 μg/mL, the cell survival rate after PFC@ $RBCM_{ICG}$ nanoparticles treatment was about 99.5%, which was higher than that after free ICG treatment (about 93.5%). The results showed that the nanoparticles can reduce the cytotoxicity of the drug (Figure 5(a)).

To evaluate the therapeutic effect of PFC@ $RBCM_{ICG}$ on tumors after irradiation with NIR laser (808 nm) when the ICG was 2.5 and 5 μg/mL. The results showed that the photodynamic effect of PFC@ $RBCM_{ICG}$ was significantly enhanced after carrying oxygen, while PLGA@ $RBCM_{ICG}$ did not have this phenomenon. In the process of the nanoparticle therapy, there are both photothermal and photodynamic effects. The oxygen-carrying PFC nanoparticles enhanced the overall therapeutic effect (Figure 5(b)). Therefore, the nanoparticles can relieve tumor hypoxia, increase ROS production, and enhance tumor photodynamic therapy effects.

3.3 Verification of the effect of erythrocyte membrane coating

Studies have shown that the mutual recognition of CD47

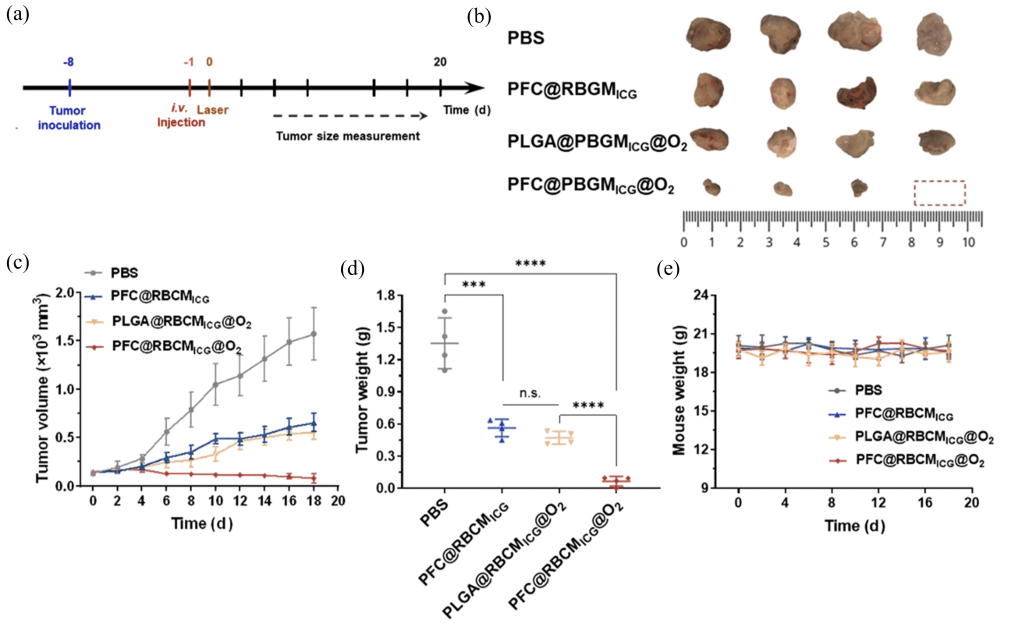

Figure 7. In vivo antitumor efficiency of PFC@ RBCM$_{ICG}$. (a) Scheme of treatment, and the tumor volume was measured every 2 days. (b) Excised tumor images. (c) Tumor volumes evolution after treatment in 20 days. (d) Weights of tumor excised after treatment. (e) Mice weight during the treatment. Data are shown as mean ±SD (n=4) $^{*}p$<0.05, $^{**}p$<0.01, $^{***}p$<0.001, $^{****}p$<0.0001.

on the cell membrane surface and SIRPα of macrophages can reduce the uptake of macrophages. Therefore, we coated the nanoparticles with red blood cell membranes, and realized the long circulation of nanoparticles in the body through this camouflage.

For 4T1 cells, there was no significant difference in the uptake of PFC@PLGA particles and PFC@RBCM particles (Figure 6(a, c)). For macrophages, the uptake of PFC@RBCM particles was much lower than that of PFC@PLGA particles (Figure 6(b, d)).

This result indicated that the coating of red blood cell membranes can effectively reduce the phagocytosis of particles by macrophages without affecting the uptake of drugs by tumor cells.

PFC@PLGA particles and PFC@RBCM particles were injected through the tail vein and tested for pharmacokinetics respectively (Figure 6(e)). The results showed that the concentration of erythrocyte membrane-coated nanoparticles was twice that of uncoated nanoparticles after 48 h (Figure 6(f)). Tumor accumulation experiments also showed that the tumor accumulation of nanomedicine wrapped in red blood cell membranes was significantly increased (Figure 6(g, h)).

3.4 In vivo antitumor efficiency of PFC@RBCM$_{ICG}$

As the method shown in Figure 7(a), the anti-tumor efficacy was further evaluated. After 20 days' regular monitor of the tumor volume, the mice were sacrificed (Figure 7(e)), and the tumor were excised (Figure 7(b)).

The PFA@ RBCM$_{ICG}$@ O$_2$ with laser administrated resulted in durable inhibition on the 4T1 tumor compared to PBS treated mice, while other nanoparticles (PFA@ RBCM$_{ICG}$, PLGA@ RBCM$_{ICG}$@ O$_2$) plus laser exerted a scant suppression on the tumor development (Figure 7(c, d)). This is because pure PFA@ RBCM$_{ICG}$ didn't have the ability to enhance the therapeutic effect, and PLGA @ RBCM$_{ICG}$ can't effectively carry oxygen. The result showed that PFA@ RBCM$_{ICG}$ carrying oxygen effectively enhanced the treatment effect.

4 Conclusions

In this work, we constructed a nanoparticle with phototherapy function to relieve the tumor hypoxia. The results proved that the nanoparticles can be effectively enriched at the tumor site, significantly increasing the production of ROS and enhancing the PDT treatment effect. At the same time, the red blood cell membrane coating can effectively reduce the uptake of the particles by macrophages and prolong the half-life in the body, so the same therapeutic effect can be achieved with lower doses. Our strategy can enhance the tumor phototherapy, reduce the toxicity to normal cells, and provide new strategies for cancer therapies.

Supplementary data

Supplementary data are available at J. Univ. Sci. Tech. China online.

Acknowledgments

This work was supported by the National Natural Science Foundation of China (31870993), the Fundamental Research Funds for the Central Universities (WK9110000005).

Conflict of interest

The authors declare no conflict of interest.

Author information

SUN Xun is currently a Master student under the supervision of Prof. YU Yue at University of Science and Technology of China. Her research mainly focuses on biomaterials.

YU Yue (corresponding author) received his PhD from Tongji Medical College of Huazhong University of Science & Technology. He is currently a professor in the Division of Life Sciences and Medicine of the University of Science and Technology of China and the chief physician of the First Affiliated Hospital of USTC.

References

[1] Tohme S, Yazdani H O, Al-Khafaji A B, et al. Neutrophil extracellular traps promote the development and progression of liver metastases after surgical stress. Cancer Research, 2016, 76 (6): 1367-1380.

[2] Day A T, Sher D J, Lee R C, et al. Head and neck oncology during the COVID-19 pandemic: Reconsidering traditional treatment paradigms in light of new surgical and other multilevel risks. Oral Oncology, 2020, 105: 8.

[3] Szakacs G, Paterson J K, Ludwig J A, et al. Targeting multidrug resistance in cancer. Nature Reviews Drug Discovery, 2006, 5 (3): 219-234.

[4] Riley R S, June C H, Langer R, et al. Delivery technologies for cancer immunotherapy. Nature Reviews Drug Discovery, 2019, 18 (3): 175-196.

[5] Hopper C. Photodynamic therapy: a clinical reality in the treatment of cancer. The Lancet Oncology, 2000, 1: 212-219.

[6] Chen J M, Fan T J, Xie Z J, et al. Advances in nanomaterials for photodynamic therapy applications: Status and challenges. Biomaterials, 2020, 237: 27.

[7] Allison R R, Moghissi K. Photodynamic therapy (PDT): PDT mechanisms[J]. Clinical Endoscopy, 2013, 46 (1): 24-29.

[8] Yang B W, Chen Y, Shi J L. Reactive oxygen species (ROS)-based nanomedicine. Chemical Reviews, 2019, 119 (8): 4881-4985.

[9] Carmeliet P, Jain R K. Angiogenesis in cancer and other diseases. Nature, 2000, 407 (6801): 249-257.

[10] Lee C, Lim K, Kim S S, et al. Chlorella-gold nanorods hydrogels generating photosynthesis-derived oxygen and mild heat for the treatment of hypoxic breast cancer. Journal of Controlled Release, 2019, 294: 77-90.

[11] Stylianopoulos T, Jain R K. Combining two strategies to improve perfusion and drug delivery in solid tumors. Proceedings of the National Academy of Sciences of the United States of America, 2013, 110 (46): 18632-18637.

[12] Phua S Z F, Yang G B, Lim W Q, et al. Catalase-integrated hyaluronic acid as nanocarriers for enhanced photodynamic therapy in solid tumor. Acs Nano, 2019, 13 (4): 4742-4751.

[13] Riess J G. Perfluorocarbon-based oxygen delivery. Artificial Cells Blood Substitutes and Biotechnology, 2006, 34 (6): 567-580.

[14] Blanco E, Shen H, Ferrari M. Principles of nanoparticle design for overcoming biological barriers to drug delivery. Nature Biotechnology, 2015, 33 (9): 941-951.

[15] Arafa M G, Mousa H A, Afifi N N. Preparation of PLGA-chitosan based nanocarriers for enhancing antibacterial effect of ciprofloxacin in root canal infection. Drug Delivery, 2020, 27 (1): 26-39.

[16] Zare E N, Jamaledin R, Naserzadeh P, et al. Metal-based nanostructures/PLGA nanocomposites: Antimicrobial activity, cytotoxicity, and their biomedical applications. Acs Applied Materials & Interfaces, 2020, 12 (3): 3279-3300.

[17] Wang L, Jiang W, Xiao L, et al. Self-reporting and splitting nanopomegranates potentiate deep tissue cancer radiotherapy via elevated diffusion and transcytosis. Acs Nano, 2020, 14 (7): 8459-8472.

[18] Jiang W, Zhang Z, Wang Q, et al. Tumor reoxygenation and blood perfusion enhanced photodynamic therapy using ultrathin graphdiyne oxide nanosheets. Nano Letters, 2019, 19 (6): 4060-4067.

[19] Gao M, Liang C, Song X J, et al. Erythrocyte-membrane-enveloped perfluorocarbon as nanoscale artificial red blood cells to relieve tumor hypoxia and enhance cancer radiotherapy. Advanced Materials, 2017, 29 (35): 7.

[20] Bahmani B, Bacon D, Anvari B. Erythrocyte-derived photo-theranostic agents: Hybrid nano-vesicles containing indocyanine green for near infrared imaging and therapeutic applications. Scientific Reports, 2013, 3: 2180.

[21] Zheng X H, Xing D, Zhou F F, et al. Indocyanine green-containing nanostructure as near infrared dual-functional targeting probes for optical imaging and photothermal therapy. Molecular Pharmaceutics, 2011, 8 (2): 447-456.

红细胞膜包被的PFC高负载的聚合物仿生纳米颗粒改善肿瘤的光疗效果

孙逊,余跃*

中国科学技术大学生命科学与医学部,中国科学技术大学附属第一医院(安徽省立医院)消化内科,安徽合肥 230001

*通讯作者. E-mail:yuyuemd@ustc.edu.cn

摘要:光动力学疗法(PDT)是一种依赖于氧气的新兴治疗手段,但是由于肿瘤部位血管供氧不足,乏氧微环境极大抑制了光动力学疗法的治疗效果.因此,如何缓解肿瘤乏氧是发展PDT的关键问题和焦点所在.全氟化碳是一类可以有效携载氧气的化合物,是目前常用的血液替代品之一.我们通过全氟化物纳米颗粒携载氧气和光热药物吲哚菁绿(ICG),并包被红细胞膜进行仿生伪装,从而降低巨噬细胞对颗粒的摄取,提高颗粒的循环能力和在肿瘤部位的富集,结合光动力疗法,有效缓解肿瘤部位乏氧情况,增强光动力效果,为肿瘤治疗提供了新思路.

关键词:药物递送系统;癌症治疗;光热疗法;光动力疗法